

Multi-Frequency Analysis of the New Wide-Separation Gravitational Lens Candidate RX J0921+4529^{1,2}

J. A. Muñoz^{3,4}, E. E. Falco³, C. S. Kochanek³, J. Lehár³, B. A. McLeod³, B. R. McNamara³, A. A. Vikhlinin³, C. D. Impey⁵, H.-W. Rix⁶, C. R. Keeton⁵, C. Y. Peng⁵ and C. R. Mullis⁷

ABSTRACT

We report the discovery of a new two-image gravitational lens candidate. The system RX J0921+4529 contains two $z_s = 1.66$ quasars separated by $6''.93$ with an H band magnitude difference of $\Delta m = 1.39$. The HST NIC2 H band images reveal an H=18.2 spiral galaxy between the quasar images, which is probably a member of a $z_l = 0.32$ X-ray cluster centered on the field. We detect an extended source near the fainter quasar image but not in the brighter image. If this extended source is the host galaxy of the fainter quasar, then the system is a binary quasar rather than a gravitational lens. VLA observations at 3.6 cm reveal emission from the lens galaxy at the flux level of 1 mJy and a marginal detection of the brighter quasar.

Subject headings: cosmology: gravitational lensing —
quasars: individual (RX J0921+4528)

1. Introduction

Gravitational lenses produced by isolated galaxies should have a mean image separation of $1''.5$, closely matching the mean separation observed in the current sample of over 60 gravitational lenses (e.g. Falco, Kochanek & Muñoz 1998). Surveys for lenses (JVAS, Patnaik et al. 1992; MG-VLA, Burke et al. 1993; CLASS, Jackson et al. 1998; see also <http://cfa-www.harvard.edu/castles>) have

¹ Based on Observations made with the NASA/ESA Hubble Space Telescope, obtained at the Space Telescope Science Institute, which is operated by AURA, Inc., under NASA contract NAS 5-26555.

² Based on observations obtained at the Multiple Mirror Telescope Observatory, a facility operated jointly by the University of Arizona and the Smithsonian Institution.

³ Harvard-Smithsonian Center for Astrophysics, Cambridge, MA 02138, USA

⁴ Instituto de Astrofísica de Canarias, E-38200 La Laguna, Tenerife, Spain

⁵ Steward Observatory, University of Arizona, Tucson, AZ 85721, USA

⁶ Max Planck Institut für Astrophysik, Heidelberg, D-69117, Germany

⁷ Institute for Astronomy, University of Hawaii, Honolulu, HI 96822, USA

demonstrated that gravitational lenses with image separations larger than $3''.0$ are rare. In order of increasing separation we know of HE 1104-1805 ($\Delta\theta = 3''.19$), MG 2016+112 ($\Delta\theta = 3''.26$) and Q 0957+561 ($\Delta\theta = 6''.26$).⁸ All three of these systems have massive early-type galaxies as their primary lens (Kochanek et al. 2000).

The overwhelming dominance of the lens population by galaxies is a consequence of the condensation of the baryons in forming galaxies. Predictions of the distribution of image separations based on the density and masses of dark matter halos, either from Press-Schechter models or simulations, catastrophically fail to match the observed separation distribution of lenses at both high and low image separations. The large separation lenses correspond to lenses produced by groups and small clusters, and Keeton (1998) has shown that we expect a strong enhancement in lensing by galaxies compared to groups and small clusters because the “cooled” baryons of the galaxies make them relatively more efficient lenses. The absolute numbers of wide separation lenses are in good agreement with predictions for power spectra normalized to produce the observed density of clusters (Narayan & White 1988, Cen et al. 1994, Kochanek 1995, Maoz et al. 1997, Wambsganss, Cen & Ostriker 1998).

Discussions of wide separation lenses were confused for many years by the presence of a larger population of binary quasars with separations of $3''.0$ to $10''.0$. Although the spectral similarities of some binary quasars remains a puzzle (e.g. Michalitsianos et al. 1997, Peng et al. 1999, Mortlock et al. 1999), Muñoz et al. (1998) and Kochanek, Falco & Muñoz (1999) demonstrated that most of the so-called “dark lenses” were binary quasars. Moreover, Kochanek et al. (1999) provided a quantitative explanation of their separations and abundances. We are now confident that wide separation lenses should be associated with visible groups or clusters of galaxies whose higher masses explain the larger separations.

In this paper we present a new example, RX J0921+4529. Its angular separation of $6''.93$ would make it the lensed quasar with the largest angular separation, if lensing were to be confirmed. The detection of a galaxy lying between the two quasars and the presence of an X-ray galaxy cluster to explain the wide separation of the images, make this system a good gravitational lens candidate. In §2 we discuss the discovery of RX J0921+4529 and subsequent observations to measure its properties. In §3 we present simple lens models and discuss their consequences.

⁸ These are the standard separations introduced by Kochanek et al. (2000) which correct for shear effects. Five lenses have *maximum* separations larger than $3''.0$. In order of increasing separation, these are HE 1104-1805 ($\Delta\theta_{max} = 3''.19$), RX J0911+0551 ($\Delta\theta_{max} = 3''.25$), HST 14176+5226 ($\Delta\theta_{max} = 3''.28$), MG 2016+112 ($\Delta\theta_{max} = 3''.88$), and Q 0957+561 ($\Delta\theta_{max} = 6''.17$). All five of these systems have massive early-type galaxies as their primary lens.

2. Observations

RX J0921+4529 was detected as an extended X-ray source in a 160 deg² ROSAT survey for high redshift galaxy clusters (Vikhlinin et al. 1998). The X-ray image was significantly ($6\text{-}\sigma$) broader than the local ROSAT Point Response Function, and the X-ray surface brightness distribution is well fit by a β -model, $S(r) = S_0/(1 + r^2/r_c^2)^{3\beta-0.5}$ with a β fixed at 0.7 and $r_c = 26''$. The X-ray flux is 2.39×10^{-13} erg/s/cm² in the 0.5-2 keV band. At the cluster redshift ($z_l \simeq 0.32$), this corresponds to $L_X = 1.0 \times 10^{44}$ erg/s ($H_0 = 50$ km s⁻¹ Mpc⁻¹), or a temperature of 3.7 keV (derived from the L_X -T relation). Optical images were obtained with the Fred Lawrence Whipple Observatory (FLWO) 1.2m telescope in the R band to search for a cluster corresponding to the X-ray source. As illustrated in Figure 1, there is a significant excess of galaxies in the field, centered on the X-ray source. The optical images also revealed two blue point sources (labeled A and B in Figure 1), which appeared to be promising quasar candidates.

We obtained spectra of the point sources (A and B) with the MMT and the Blue Channel spectrograph. The spectra had integration times of 3000s and 3600s respectively, and they covered a wavelength range of 3230–8800Å, with a resolution of 1.96 Å pixel⁻¹ and an effective resolution (FWHM) of 7 Å. Both A and B are $z_s = 1.66$ quasars (see Figure 2), with a velocity difference of $|\Delta v| \leq 1500$ km s⁻¹ depending on the wavelength range used for the spectral cross-correlation. Thus, RX J0921+4529A/B are either a gravitational lens or a binary quasar. For a lens with a time delay ~ 100 days, a velocity difference of $|\Delta v| \sim 1500$ km s⁻¹ could be created by quasar variability coupled with a long time delay (see Small, Sargent & Steidel 1997). Note that the continuum of the B spectrum is flatter than that of the A spectrum. In addition to the two quasars, spectra were obtained for 5 of the nearby galaxies (see Table 2). Three of them were acquired at the University of Hawaii 2.2m telescope. All five were found to have redshifts of $z_l \simeq 0.32$, confirming the presence of a cluster and a favorable geometry for producing a wide separation lens. We failed to measure the redshift of the central, putative lens galaxy G, and we will assume it is a member of the cluster.

We obtained HST observations of RX J0921+4529, as part of the CASTLES (CfA/Arizona Space Telescope Lens Survey) project. The target was observed for 2560s using the NICMOS/NIC2 camera with the F160W filter (H-band), and for 1800s using the WFPC2 camera with the F814W filter (I-band). The data were reduced and analyzed using the standard procedures described in Lehar et al. (2000), see also McLeod (1997). In the H-band image the A and B quasars are separated by $6''.929 \pm 0''.006$ and have H-band magnitudes of 16.90 ± 0.03 and 18.29 ± 0.04 respectively. Figure 3 shows the surrounding field from the NICMOS H-band image. Lying between the two quasars is an $H=18.2 \pm 0.4$ ($I-H=1.9 \pm 0.4$) galaxy with apparent spiral structure (see Figure 4 and Table 1). All other wide separation lenses have a massive early-type galaxy which dominates the lensing effects. In the residual image found after subtracting the two quasars from the NIC2 H-band image (see Figure 4), there appears to be an extended, faint object B' near the fainter quasar B. In our best models there is a small but poorly determined shift ($0''.3 \pm 0''.2$) between B' and B, suggesting that B' is a faint cluster galaxy. However B' is undetected in the

I-band image and we cannot rule out that it corresponds to the host galaxy of the B quasar. No comparable extended object is seen near the A quasar. As we discuss in §3, if B' is the host galaxy of quasar B, the absence of a host galaxy for quasar A means that the system is a perversely located binary quasar rather than a gravitational lens.

We cataloged the galaxies in the HST images using the SExtractor package (Bertin & Arnouts 1996). The software classified the optical objects, and computed total magnitudes using Kron-type automatic apertures. Colors were computed using fixed apertures scaled to the F814W size of each object. Table 2 lists all the galaxies detected by HST within 20'' of the lens, after visually confirming the SExtractor classification. The galaxies were labeled G# in order of decreasing I-band brightness, or H# for those NICMOS galaxies with no I-band detection. The large number of galaxies detected corroborates the presence of the cluster of galaxies. Figure 5 shows HST colors and magnitudes for the nearby galaxies, compared to evolutionary tracks for various spectrophotometric models (Bruzual & Charlot 1993; 2000, in preparation). The putative lens galaxy G and its neighbors are photometrically consistent with the $z = 0.32$ cluster redshift. Galaxy G appears to have spiral structure (see Figure 4) which our image fitting software is not designed to model. We modeled the galaxy (Table 1) as a de Vaucouleurs bulge plus an exponential disk, but the residuals are still large. Because the galaxies in this field are larger than most in the CASTLES target fields, we have increased the color apertures to a fixed 4'' diameter in all cases.

Finally, we obtained a radio map of RX J0921+4529, using the VLA C configuration at 3.6 cm. The VLA observations were made on 1998.12.10, with 15 minutes on target. The beam FWHM was 3'' and the detection limit was 0.05 mJy/beam. The cluster galaxy G2 was clearly detected, so we aligned the optical and radio images using it. In the VLA map (see Figure 6), both G2 and the lens galaxy G have 8.5 GHz fluxes of $\simeq 1.0 \pm 0.1$ mJy. There may be a marginal detection of A, at $\simeq 0.1 \pm 0.05$ mJy. If A is a 0.1 mJy source, then we would expect B to be a ~ 0.03 mJy source, so a deeper radio image could further confirm the lensing nature of the system.

3. Discussion

With a separation of 6''.93, RX J0921+4529 is the widest angular separation lens found without searching directly behind a rich cluster. Almost all the data support the lens interpretation, as we see 2 images of a $z_s = 1.66$ lensed quasar with similar spectra and a modest magnitude difference. There is a foreground galaxy located between the quasars to provide the high surface density region needed to produce two images, and the galaxy is almost certainly a member of the $z = 0.32$ X-ray cluster which provides the additional mass needed to produce the large separation.

The large angular separation of RX J0921+4529 should be produced by the combination of the main lens galaxy lying between the two quasar images and the presence of the galaxy cluster. We estimated the local tidal shear from nearby galaxies by assuming that each is embedded in

a singular isothermal sphere halo, with the same mass-to-light ratio as the lens galaxy G. We assumed an Einstein ring radius of $b \sim 1''$ for the lens galaxy, and scaled the other galaxy ring sizes to the SExtractor I-filter luminosity, with $b \propto \sqrt{L}$ (see Table 2). A total $\gamma_T \simeq 0.17$ in the direction $\text{PA} = -36^\circ$ is obtained by taking the tensor sum of the individual contributions. Because the HST field is not big enough to include the full cluster this shear estimate represents only a preliminary value. Chandra or XMM imaging and deeper wide-field optical images could clarify the cluster properties and its contribution to the lensing gravitational potential.

The simplicity of the lens geometry means that we find a wide range of lens models consistent with our current data. However with the extant data, we cannot determine the position of the cluster center, and we cannot easily include the cluster in the lens models. Thus, our objective in this section is only to illustrate the importance of the interpretation of B' as either a small cluster galaxy or the host of the B quasar. For now we fit the system only with a singular isothermal sphere (SIS) and an external shear. Given the lens galaxy and quasar positions, and the quasar flux ratio (see Table 1) this lens model needs an Einstein radius $b = 3''.3$, and an external shear $\gamma = 0.047$ orientated in the direction $\text{PA} = 33^\circ$. The leading image is the fainter B quasar and the time delay in a flat ($\Omega = 1$) cosmology is $\Delta t = 93 h^{-1}$ days⁹. In Figure 7 we show both the source and lens planes. The source plane includes an image of the lens galaxy G to orient the figure, a point source for the quasar and its host galaxy with a de Vaucouleurs profile. In the image plane we see the 2 images of the quasar which exactly fit the observed positions and fluxes. The small arc from the host galaxy near quasar B has a flux matching that of B'. However, if B' were a host galaxy, we would see the larger, brighter and undetected arc seen near image A.

We are reasonably certain that the extended object B' near the B quasar is a faint cluster galaxy rather than the host galaxy of quasar B. If, however, it is the host galaxy, the absence of a larger host image near quasar A means that the system is a particularly perverse example of a binary quasar lying behind a foreground X-ray cluster. Deeper HST images would determine more accurately the B' position and would clarify the nature of the object. Deeper radio images may also resolve the problem if our marginal detection of the A quasar at 8.5 GHz is real.

Acknowledgements: Support for the CASTLES project was provided by NASA through grant numbers GO-7495 and GO-7887 from the Space Telescope Science Institute which is operated by the Association of Universities for Research in Astronomy, Inc. under NASA contract NAS 5-26555. This research was supported in part by the Smithsonian Institution. CSK is also supported by NASA grant NAG5-4062.

⁹A singular isothermal ellipsoid (SIE) with a fixed external shear to the observed values (see above) also fits the data with the lens parameters $b = 3''.3$, $e=0.48$ and $\theta_e = 51^\circ$. For this model the time delay is $\Delta t = 118 h^{-1}$ days.

REFERENCES

- Bertin, E. & Arnouts, S. 1996, *A&AS*, 117, 393
- Bruzual, A.G. & Charlot, S. 1993, *ApJ*, 405, 538
- Bruzual, A.G. & Charlot, S. 2000, in preparation
- Burke, B.F., Conner, S.R., Hewitt, J.N. & Lehár, J. 1993, in “Sub-arcsecond Radio Astronomy”, Eds R.J. Davis, R.S. Booth (Cambridge:CUP), p.123
- Cen, R., Gott, J.R., Ostriker, J.P. & Turner, E.L. 1994, *ApJ*, 423, 1
- Falco, E.E., Kochanek, C.S. & Muñoz, J.A. 1998, *ApJ*, 494, 47
- Jackson, N., Helbig, P., Browne, I., Fassnacht, C.D., Koopmans, L., Marlow, D. & Wilkinson, P.N. 1998, *A&A*, 334, 33
- Keeton, C.R. 1998, PhD thesis, Harvard University
- Keeton, C.R., Kochanek, C.S., & Falco, E.E. 1998, *ApJ*, 509, 561
- Kochanek, C.S. 1995, *ApJ*, 453, 545
- Kochanek, C.S., Falco, E.E., & Muñoz, J.A., 1999 *ApJ*, 510, 590
- Kochanek, C.S., Falco, E.E., Impey, C.D., Lehár, J., McLeod, B.A., Rix, H.-W., Keeton, C.R., Muñoz, J.A. & Peng, C.Y. 2000, *ApJ*, in press, astro-ph/9909018
- Lehár, J., C.S., Falco, E.E., Kochanek, C.S., McLeod, B.A., Muñoz, J.A., Impey, C.D., Rix, H.-W., Keeton, C.R. & Peng, C.Y. 2000, *ApJ*, 536, 584
- Maoz, D., Rix, H.-W., Gal-Yam, A. & Gould, A. 1997, *ApJ*, 486, 75
- McLeod, B. 1997, in 1997 HST Calibration Workshop, eds. S. Casertano, R. Jedrzejewski, C.D. Keyes, M. Stevens, 281
- Michalitsianos, A.G., Falco, E.E., Muñoz, J.A. & Kazanas, D. 1997, *ApJ*, 487, L11
- Mortlock, D. J., Webster, R. L. & Francis, P. J. 1999, *MNRAS*, 309, 836
- Muñoz, J. A., Falco, E. E., Kochanek, C.S. et al. 1998 *ApJ*, 492, L9
- Narayan, R. & White, S. 1988, *MNRAS*, 231, 97
- Patnaik, A.R., Browne, I.W.A., Wilkinson, P.N. & Wrobel, J.M. 1992, *MNRAS*, 254, 655
- Peng, C.Y., Falco, E.E., Impey, C.D., Kochanek, C.S., Lehár, J., McLeod, B.A., Rix, H.-W., Keeton, C.R. & Muñoz, J.A. 1999, *ApJ*, 524, 572
- Small, T.A., Sargent, W.L. & Steidel. CC. 1997, *AJ*, 114, 2254
- Vikhlinin, A. A., et al. 1998, *ApJ*, 502, 558
- Wambsganss, J., Cen, R. & Ostriker, P. 1998, *ApJ*, 494, 29

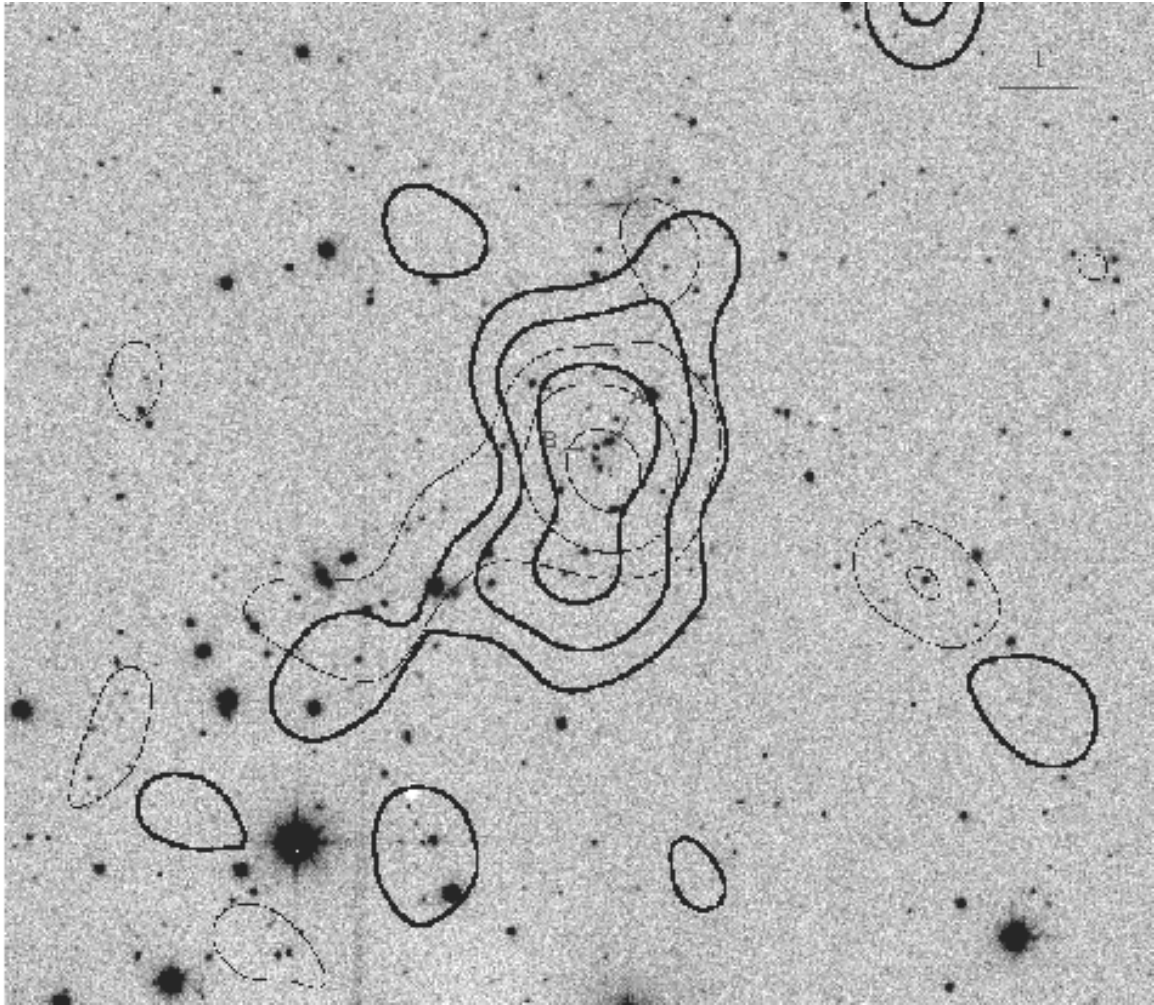


Fig. 1.— R-band image obtained with the FLWO 1.2m telescope. The thin contours are the number density of optical galaxies (constant linear step of 1.37 per arcmin²) and the thick contours are the X-ray brightness, smoothed with a 30'' FWHM Gaussian (the surface brightness contours are spaced by factors of 2).

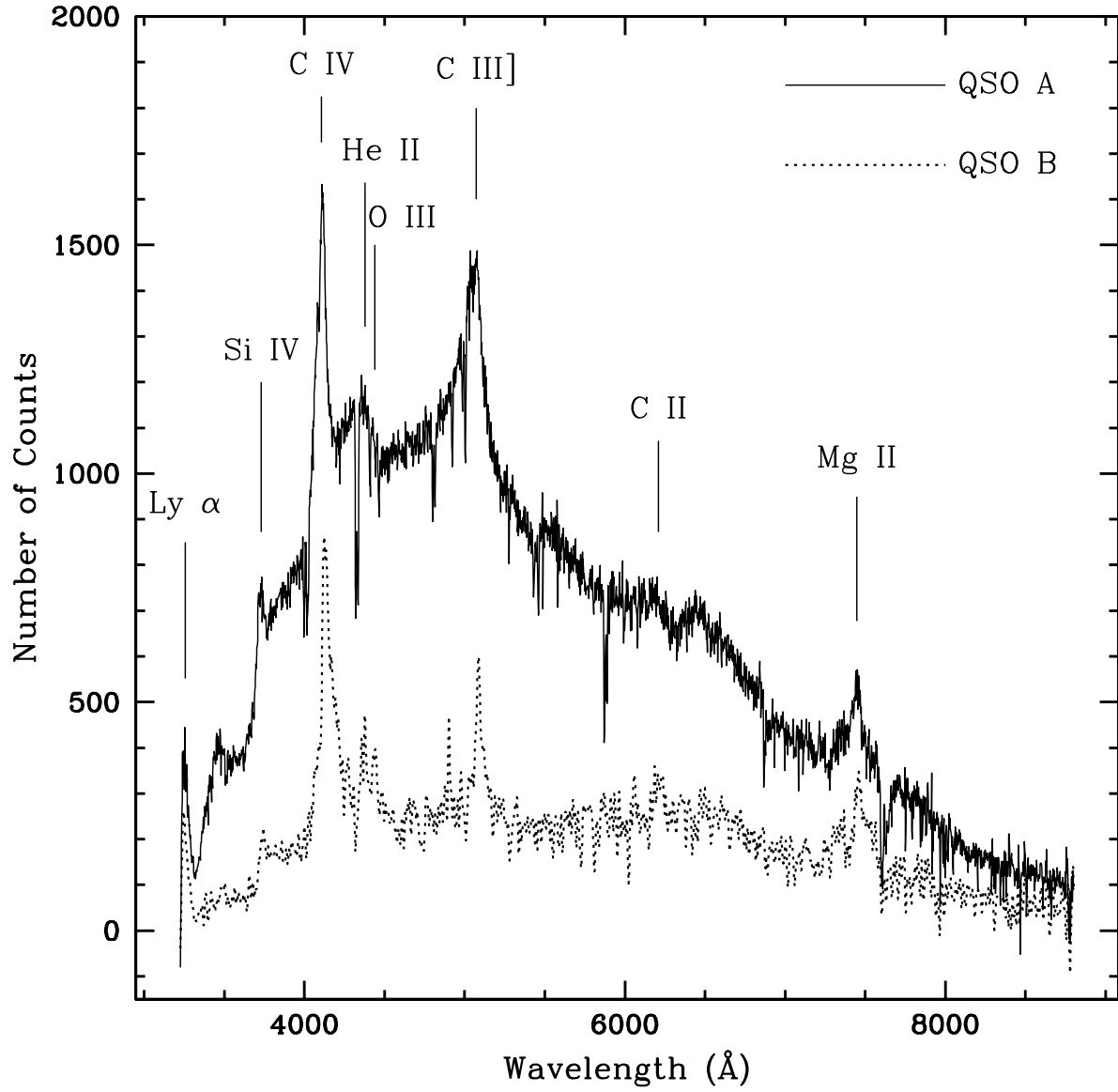


Fig. 2.— Spectra of RX J0921+4529 A and B. The solid (dashed) line corresponds to the A (B) component. The B spectrum is multiplied by a factor 2 for display purposes. Prominent emission lines are labeled.

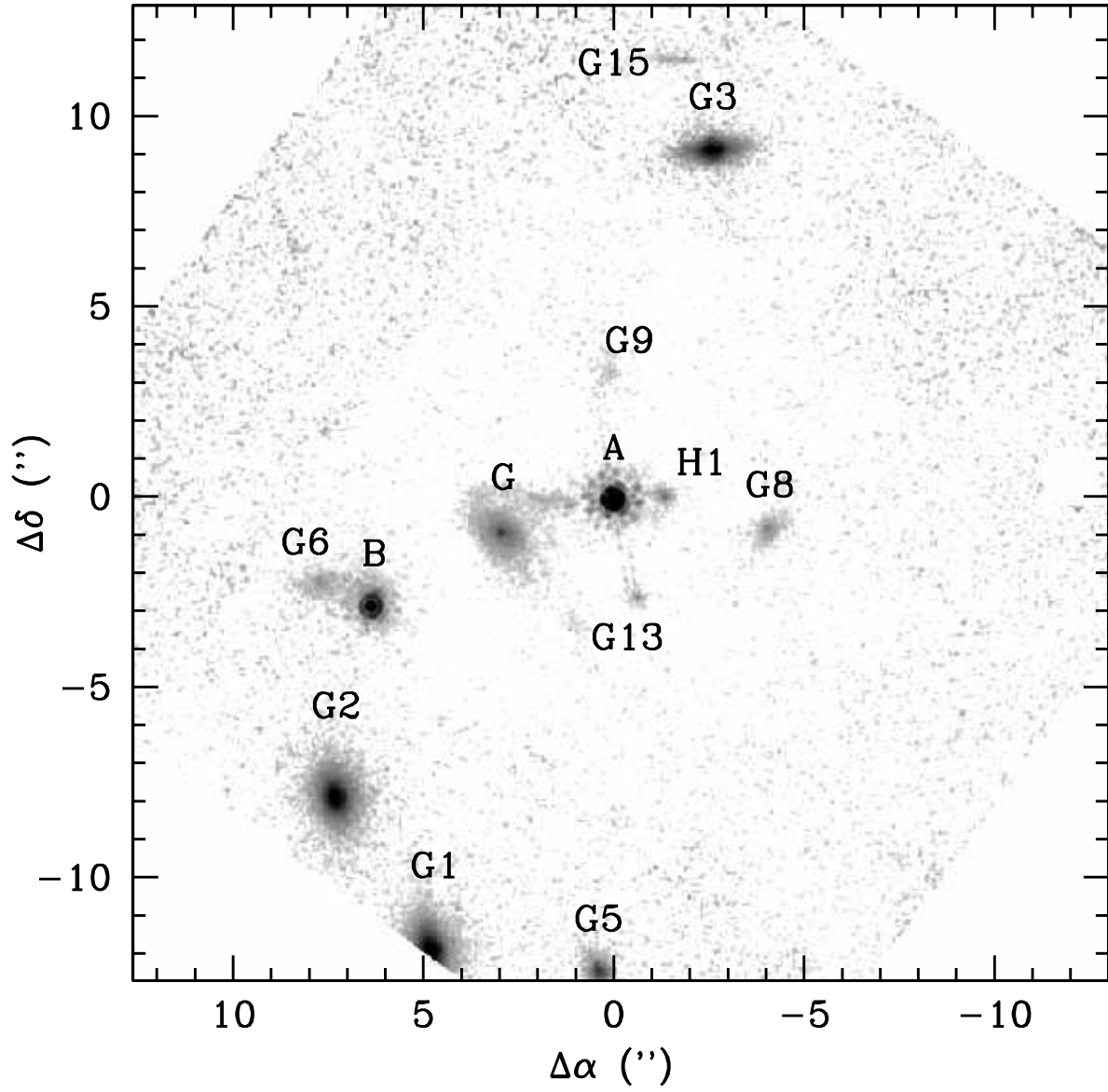


Fig. 3.— The complete NIC2 image centered on the A quasar (RA 09h 21m 12.81s, DEC +45° 29' 04".4 (J2000)). The two quasar components A and B, the galaxy lens G and some nearby galaxies are labeled (see Table 2).

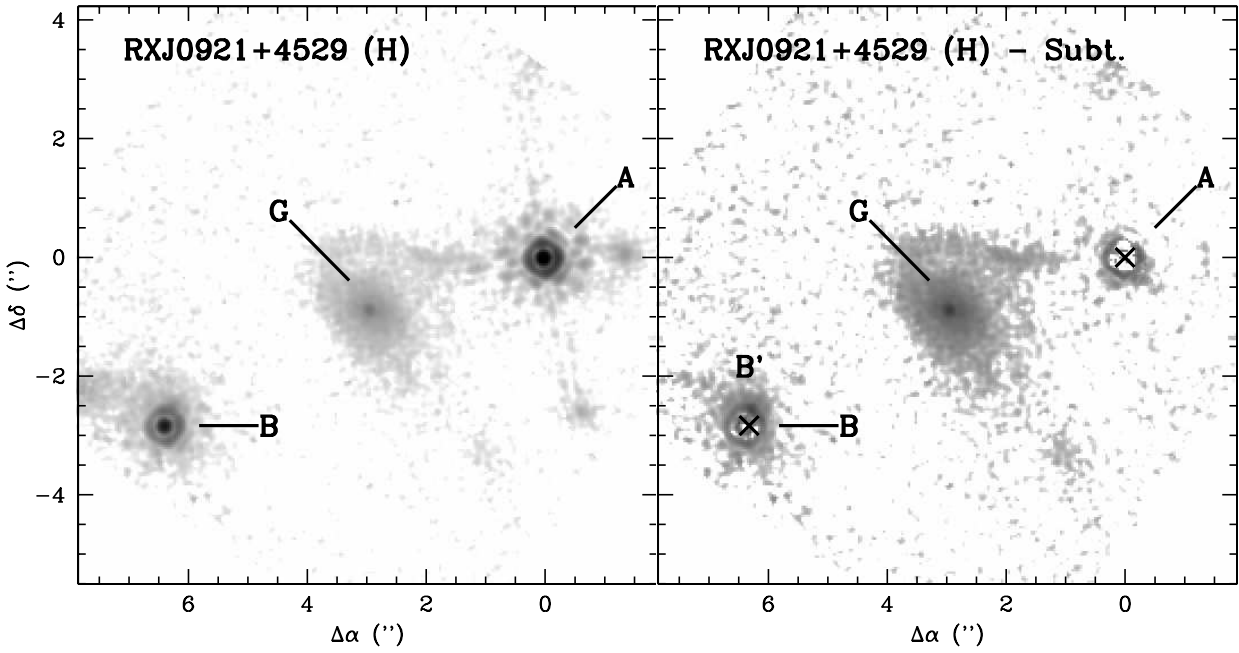


Fig. 4.— The left panel shows the HST NIC2 observed image and the right panel shows the residuals after quasar subtraction. Quasar images A & B and lens galaxy G are labeled. The B quasar subtraction reveals the B' extended faint object .

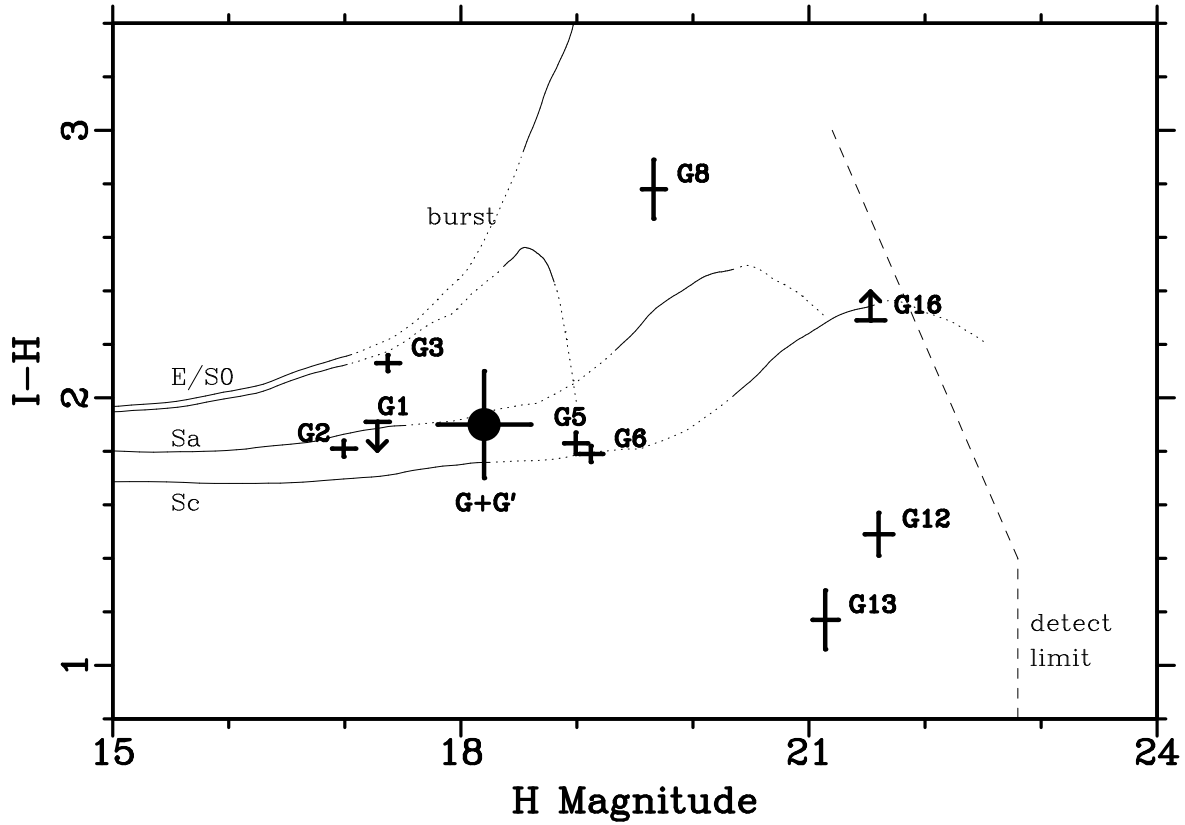


Fig. 5.— HST Colors and total magnitudes for the lens galaxies and their neighbors. The curves show photometric evolution models for L_* galaxies, alternating between solid and dotted lines at intervals of $\Delta z = 0.5$. Galaxies with $L < L_*$ should be shifted to the right of the color-mag curve which corresponds to their morphology type. The H-band magnitudes have been offset by 0.5 mag, to correct for the SExtractor aperture error (Lehár et al. 2000). The best-fit component photometry for G+G' (see text and Table 1) is shown as a filled circle.

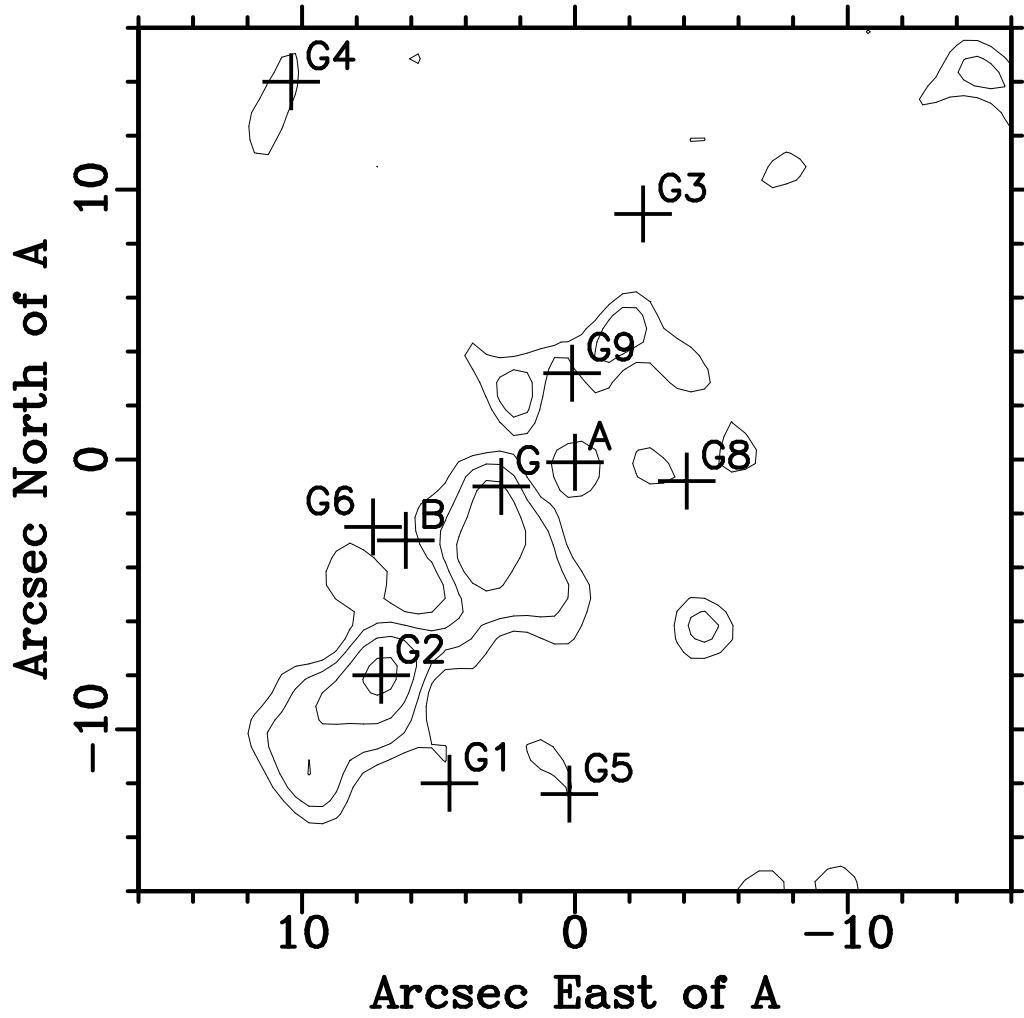


Fig. 6.— VLA C-array map of RX J0921+4529 at 3.6 cm. The beam size is approximately $3''$ (FWHM), and the radio contours increase by factors of $\sqrt{2}$, from twice the off-source rms noise ($46 \mu\text{Jy/beam}$). Positions of the brightest optical objects are shown.

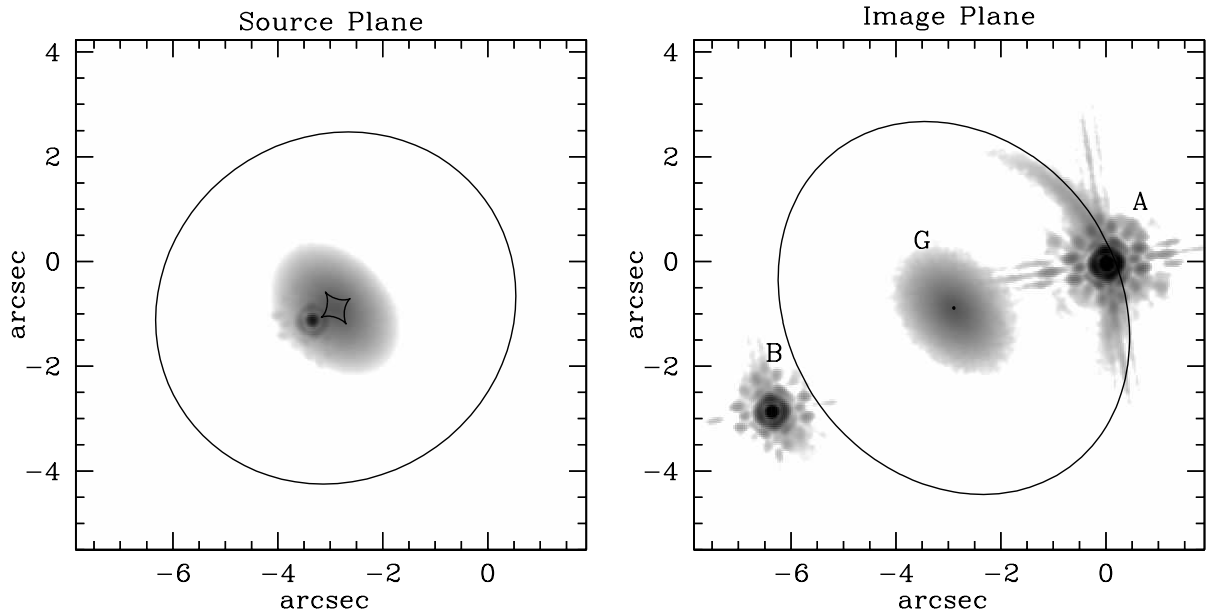


Fig. 7.— The source plane (left) includes an image of the lens galaxy G to orient the figure, a point source for the quasar and its host galaxy with a de Vaucouleurs profile. In the image plane (right) we see the 2 images of the quasar which exactly fit the observed positions and fluxes. The small arc from the host galaxy near quasar B has a flux matching that of B'. However, if B' is a host galaxy, then we should see the larger, brighter and undetected arc seen near image A. The caustic and critical lines are shown in the source and image plane respectively.

Table 1. HST Astrometry and Photometry of RX J0921+4529

ID	RA "	Dec "	Magnitude H	Color I–H	$R_e^{(1)}$ "	$1 - b/a$	PA deg
A	$\equiv 0$	$\equiv 0$	16.90 ± 0.03	1.06 ± 0.05			
B	6.322 ± 0.005	-2.837 ± 0.004	18.29 ± 0.04	1.65 ± 0.05			
B'	6.22 ± 0.05	-2.6 ± 0.2	18.8 ± 0.7	> 2.4	1.0 ± 0.3	0.3 ± 0.4	0 ± 50
G	2.908 ± 0.015	-0.881 ± 0.006	18.6 ± 0.2	1.6 ± 0.2	0.68 ± 0.13	0.48 ± 0.09	29 ± 5
G' ⁽²⁾	2.908 ± 0.015	-0.881 ± 0.006	19.4 ± 1.2	2.8 ± 1.7	0.5 ± 0.3	0.4 ± 0.2	75 ± 20

Note. —

⁽¹⁾ R_e is the effective radius of the de Vaucouleurs profiles for B' and G', and the scale radius of the exponential disk for G.

⁽²⁾ Due to the complex morphology of the galaxy lens we fit it simultaneously with a de Vaucouleurs (G') and an exponential disk (G) profile to account for as much of the galaxy flux as possible. Note that in the text, we refer to the flux of G as the sum of the fluxes of these two components.

Table 2. Nearby Objects

ID	ΔRA	ΔDec	I	I-H	γ	θ_γ	Notes
A	0.0	0.0	18.21 ± 0.10	1.31 ± 0.03		-73	$z=1.66$
B	6.3	-2.9	19.91 ± 0.10	1.76 ± 0.03		-59	$z=1.66$
G	2.7	-0.9	20.15 ± 0.10	1.60 ± 0.03			
G1	4.6	-11.8	19.13 ± 0.10	< 1.91	0.072	-9	on NIC2 edge
G2	7.1	-7.9	19.16 ± 0.10	1.81 ± 0.03	0.096	-31	$z=0.3194 \pm 0.0008$
G3	-2.5	9.2	19.88 ± 0.10	2.13 ± 0.03	0.049	-28	$z=0.31 \pm 0.01$
G4	10.4	14.1	20.91 ± 0.10		0.021	27	
G5	0.2	-12.3	21.32 ± 0.10	1.83 ± 0.04	0.025	13	
G6	7.5	-2.4	21.41 ± 0.10	1.79 ± 0.03	0.058	-72	
G7	20.4	0.1	21.83 ± 0.10		0.013	87	
G8	-4.1	-0.7	22.32 ± 0.10	2.78 ± 0.11	0.026	-88	
G9	0.1	3.3	22.98 ± 0.11	0.66 ± 0.14	0.027	-33	
G10	17.3	1.6	22.99 ± 0.12		0.009	80	
G11	10.5	-16.0	23.23 ± 0.13		0.007	-27	
G12	0.9	-3.4	23.64 ± 0.12	1.49 ± 0.08	0.032	39	
G13	-0.7	-2.6	24.18 ± 0.13	1.17 ± 0.11	0.020	65	
G14	8.3	6.5	24.43 ± 0.13	> 3.62	0.008	36	
G15	-1.4	11.6	24.75 ± 0.15	> 3.66	0.005	-19	
G16	-14.9	0.2	24.97 ± 0.15	> 2.29	0.003	-87	
H1	-1.3	0.1		> 7.38	0.047	-77	$H=20.42 \pm 0.10$
T1	54.0	-50.7	18.32 ± 0.10		0.016	-46	$z=0.3179 \pm 0.0004$
T2	-1.4	-30.7	18.53 ± 0.10		0.035	8	
T3	22.5	-22.1	18.95 ± 0.10		0.030	-43	$z=0.309 \pm 0.001$
T4	10.9	-49.3	18.99 ± 0.10		0.017	-9	$z=0.319 \pm 0.001$

Note. — SExtractor position offsets from A are given in arcseconds. Galaxies on the WFPC2 image within $20''$ of G are labeled Gx , and those detected only with NIC2 are labeled Hx . Galaxies outside of $20''$ with large estimated shears are included as Tx . Tidal shear estimates γ assume SIS halos with the same redshift and mass-to-light ratio as G, and the shear position angles θ_γ are in degrees CCW from North.